Chemosphere, Volume 281, October 2021, Article number 130986
DOI: 10.1016/j.chemosphere.2021.130986

Understanding the mechanisms of biological struvite biomineralisation

Authors: Yirong Leng, Ana Soares*

Cranfield Water Science Institute, Cranfield University, Bedfordshire, MK43 0AL, UK

* Corresponding author at Cranfield Water Science Institute, Cranfield University, Vincent Building, Cranfield, Bedfordshire, MK43 0AL, UK. Tel.: +44 (0) 1234 758121. E-mail address: a.soares@cranfield.ac.uk.

Abstract

The mechanisms of struvite production through biomineralisation were investigated for five microorganisms (*Bacillus pumilus*, *Brevibacterium antiquum*, *Myxococcus xanthus*, *Halobacterium salinarum* and *Idiomarina loihiensis*). After 72–96h of incubation, the microbial strains tested increased the solution pH from 7.5–7.7 to 8.4–8.7, and removed ortho-phosphate (63–71%) and magnesium (94–99%) by biomineralisation. The minerals formed were identified as struvite (i.e. bio-struvite). Within the initial 24h of incubation, microbial growth rates of 0.16–0.28 1/h were measured, and bio-struvite production was observed when the solution supersaturation index with respect to struvite achieved 0.6–0.8 units. The crystals produced by *B. pumilus*, *H. salinarum* and *M. xanthus* were thin trapezoidal-platy shaped and presented a gap size about 200 μm for intervals between cumulative volume undersize distribution at 50% and 90%. While *B. antiquum* and *I. loihiensis* produced crystals of coffin-lid/long-bar shape and a narrow size gap around 100 μm for intervals between cumulative volume percentage of 50% and 90%, indicating homogeneous crystal size distribution. Intracellular supersaturation of struvite phase was achieved within *B. antiquum* and *I. loihiensis* cells, corresponding to observation of intracellular vesicle-like structures occupied with electron-dense granules/materials. This study suggests that *B. antiquum* and *I. loihiensis* produced bio-struvite through biologically controlled mineralization. This mechanism is the preferred for recovering nutrients from streams such as wastewater because it allows a link between manipulation of microbial growth conditions and bio-struvite production, even in highly complex streams like wastewater.

Keywords: biomineralisation; bio-struvite; phosphorus recovery; intracellular cluster

Published by Elsevier. This is the Author Accepted Manuscript issued with: Creative Commons Attribution Non-Commercial No Derivatives License (CC:BY:NC:ND 4.0). The final published version (version of record) is available online at DOI:10.1016/j.chemosphere.2021.130986. Please refer to any applicable publisher terms of use.

1. Introduction

The formation of struvite (magnesium ammonium phosphate hexahydrate, $MgNH_4PO_4.6H_2O$) via biomineralisation was identified as a result of the metabolism of nitrogenous-rich organic matter such as urease and proteins by key microorganisms. This results in the release of ammonia (NH_4-N), which increases the solution pH and, in the right conditions, leads to the formation of struvite (Sadowski et al., 2014; Sinha et al., 2014). The biological production of struvite (i.e. bio-struvite) has been suggested as a key route to recover phosphorus (P) and nitrogen (N) from wastewater, with advantages of no pH-adjustment and recovering P even at low ortho-phosphate (PO_4-P) concentrations (e.g. 7.5 mg/L) when compared with conventional chemical ways (Doyle and Parsons, 2002; Soares et al., 2014). A wide spectrum of microorganisms have been reported to be capable of producing bio-struvite in controlled conditions (i.e. synthetic media) and wastewater streams (González-Muñoz et al., 2008; Grover et al., 1997; Sinha et al., 2014; Soares et al., 2014). Furthermore, microbial activity may exert influence on the formation, growth and morphology of bio-struvite, such that the cations interact with the negatively charged cell outer layer (Frankel and Bazylinski, 2003; Schultze-Lam et al., 1996).

Biomineralisation is based on cellular control of the process and is traditionally grouped into two distinct mechanisms: biologically induced mineralisation (BIM) and biologically controlled mineralisation (BCM) (Mann, 2001). BIM takes place in an open environment where the minerals are precipitated adventitiously and their chemical characteristics could be readily altered by interference from foreign substances and interactions between various metabolic pathways (Mann, 2001). BCM encompasses genetic control where microorganisms can exert specific regulation in isolated compartments to, for example, control solution composition within membrane-bound lipid vesicles (Mann, 2001; Weiner and Dove, 2003). Distinctive features of BCM include biominerals' species-specific crystallochemical properties and their homogeneity with respect to morphology, size, composition (Mann, 2001). Thus, BCM has potential to yield reproducible products of more controlled quality. Nevertheless, struvite formation through BCM has been scarcely reported. Only three bacteria, *Paramecium tetraurelia*, *Brevibacterium antiquum* and *Enterobacter sp*, have been reported to be involved in BCM bio-struvite formation, as determined by either the occurrence of intracellular bio-

struvite (Grover et al., 1997; Smirnov et al., 2005), or by morphological, compositional and minerological heterogeneity in the struvite crystals (Sinha et al., 2014).

All microorganisms selected in this study have been proven to form bio-struvite in streams (e.g. synthetic solution, wastewater), but the mechanisms have not yet been documented in detail. *B. antiquum* was reported to grow in Mg^{2+}- and PO_4-rich synthetic solutions and produce bio-struvite crystals within the cytoplasm, aligning to the BCM mechanism (Smirnov et al., 2005). The *Myxococcus xanthus* bio-struvite was found related to autolysis of cellular membranes in synthetic solutions (Da Silva et al., 2000). *Halobacterium salinarum* and *Bacillus pumilus* bio-struvite were observed in wastewater streams (Soares et al., 2014), and *Idiomarina loihiensis* bio-struvite was observed in seawater synthetic solutions (González-Muñoz et al., 2008). This study aims at understanding the mechanisms involved in bio-struvite formation through exploring the relationships between cell growth, solution composition, crystallization properties, microbial activity and specific cell structures, for selected microorganisms. Based on the authors' knowledge, this is the first study to investigate the mechanisms of biomineral formation for the *H. salinarum*, *B. pumilus* and *I. loihiensis.*

2. Material and methods

2.1 Microorganisms and microbial cultivation

Five microbial strains, initially isolated from soil or marine environments, were purchased from commercial culture collections: *H. salinarum* (DSM 671, German Resource Centre for Biological Material, Germany), *B. pumilus* (GB43, LGC Standards, Middlesex, UK), *B. antiquum* (DSM 21545, German Resource Centre for Biological Material, Germany), *M. xanthus* (CECT 422, Spanish Type Culture Collection, University of Valencia, Paterna, Spain) and *I. loihiensis* (MAH1 /CECT 5996, Spanish Type Culture Collection, University of Valencia, Paterna, Spain).

I. loihiensis was grown in 300 mL glass bottles (Poulten Graf™, Fisher Scientific, UK) containing 90 mL synthetic B41 media (4 g/L yeast extract, 2 g/L magnesium sulphate heptahydrate - $MgSO_4 \cdot 7H_2O$ and 2 g/L di-potassium hydrogen phosphate - K_2HPO_4) (Da Silva et al., 2000) with additional 1% sodium chloride (NaCl) (González-Muñoz et al., 2008). The other four microorganisms were grown in synthetic B41 media without NaCl. The autoclaved

media (121°C, 20 min) were inoculated with 10 mL of pre-washed (0.9% w/v NaCl) microbial cultures grown for 96 h. The bottles were capped with foam stoppers and incubated on an orbital shaker (Stuart model SSL1, Fisher Scientific, UK) at agitation rate 150 RPM at room temperature (22–24°C) for 96 h. Samples (sacrificial bottles) were taken at regular intervals (approximately every 12 h), and the entire content of the bottles was analysed to avoid biased analysis, specifically when completing the crystal size distribution analysis. All tests were completed in duplicate, and controls were maintained under identical conditions but without inoculation.

2.2 Isolation, purification and determination of precipitants; abiotic struvite preparation

At the end of the incubation period, the precipitated crystals were filtered through a 10 µm nylon-mesh filter (Plastok, UK) and washed with deionized (DI) water. The filter was air-dried at 37°C for 4 h and weighed to determine the crystal production yield.

Abiotic struvite was prepared in a chemical way, by mixing 200 mL 50 mM $MgSO_4 \cdot 7H_2O$ solution (pre-adjusted to pH 9 with 1 M sodium hydroxide) with 100 mL 0.2 M $NH_4H_2PO_4$ (pre-adjusted to pH 9 with 1 M sodium hydroxide) (Le Corre et al., 2005), and left shaking on an orbital shaker at 150 RPM at room temperature for 24 h.

2.3 Supersaturation index and intercellular crystals

Supersaturation index of struvite ($SI_{struvite}$) was determined by Visual MINTEQ ver. 3.1 (Gustafsson, 2000), which uses chemical equilibrium models based on the thermodynamic equilibrium and a solubility product constant (K_{sp}) of $10^{-13.26}$ (Ali et al., 2005). Assuming no loss of bio-struvite crystals in filtration, K_2HPO_4 was the only P resource and $MgSO_4 \cdot 7H_2O$ was the only Mg^{2+} resource in solution for bio-struvite, cell structures and intracellular ions of PO_4-P and Mg^{2+}, and the intracellular ion concentrations of PO_4-P and Mg^{2+} were estimated by a mass balance (Eq. 1–2):

$$PO_4\text{-}P_{\ removed\ from\ solution} = PO_4\text{-}P_{\ crystals} + P_{\ cell\ structures} + PO_4\text{-}P_{\ intracellular} \quad \text{(Equation 1)}$$

$$Mg^{2+}_{\ removed\ from\ solution} = Mg^{2+}_{\ crystals} + Mg^{2+}_{\ cell\ structures} + Mg^{2+}_{\ intracellular} \quad \text{(Equation 2)}$$

To estimate the intracellular supersaturation, the volume and dry weight (DW) of each single cell were assumed to be between 0.5–2 × 10^{-15} L (Gao, 2008) and 1.6–2.8 × 10^{-13} g (Logan, 2008, 2005), respectively. Magnesium and P were assumed to account for 0.5% and 3% of microbial cells on a DW basis, respectively (Stolp, 1988). There was no significant loss of Mg and P by extracellular materials such as eDNA or polyphosphate during microbial growth and activity. Furthermore, a constant NH_4-N concentration of 1 mM within cells was assumed; as well as equal distribution of PO_4-P and Mg^{2+} ions in the cytoplasm; a constant degree of intracellular $SI_{struvite}$ during the incubation period; and intracellular neutral pH of 7 for *H. salinarum, M. xanthus, B. antiquum* and *B. pumilus* and mild alkaline pH of 8 for *I. loihiensis* (Leng et al., 2020). The mass balance of NH_4-N cannot be completed in this study due to loss of nitrogen caused by volatilization of ammonia from crystalline frameworks of bio-struvite during air-drying.

For examining intracellular crystals, the microbial cells were harvested from stationary cultures (60 h) and diluted with DI water to achieve approx. 200–300 cell/μL. A drop of the diluted culture was transferred to a 400-mesh Formvar and carbon-coated copper grid, air-dried and examined by transmission electron microscopy (TEM, CM 20, Philips, Japan).

2.4 Analytical methods

Over the incubation period, intact cell counts were estimated using a flow cytometer (BD accuri C6, BD Biosciences, US) by the SYBR Green I (SG) - propidium iodide (PI) co-staining method (Nocker et al., 2017). Solution pH values were determined by using a digital pH-meter (Jenway 3540, Bibby Scientific, UK). Followed by 0.22 μm sterile filtration (Sartorius Stadium Biotech, Germany), the concentrations of soluble chemical oxygen demand (SCOD), PO_4-P and NH_4-N were analysed using a Spectroquant® test kit (Merck, Germany) according to the manufacturer's instructions. Magnesium and potassium (K^{+}) were analysed by atomic absorption spectroscopy equipped with flaming and electrothermal spectrometers (AAS, Analyst 800, PerkinElmer, UK).

The crystal growth was investigated over time by frequent particle size distribution (D_v) analysis using a Mastersizer 3000 (Hydro EV, Malvern Instruments Ltd, UK). Microbial distribution and crystal morphology in fresh culture was recorded by microscopic analysis using an optical microscope (Division of GT vision Ltd, UK). Morphology and surface

characteristics of the isolated purified crystals were investigated by using a scanning electron microscope (SEM) equipped with energy dispersive X-ray spectroscopy (SEM-EDX, XL 30 SFEG, Philips, The Netherlands). Crystal characterizations of the isolated purified crystals were identified by XRD (D5000, Siemens / Bruker, Germany) and compared with the standard curve of struvite (pattern COD 9007674). Element analysis of the precipitants was implemented through dissolving 25 mg of the precipitations in 20 mL extra pure water (pre-adjusted to pH 2 by 1 M hydrogen chloride), followed by 0.22 μm filtration to determine PO_4-P, NH_4-N, Mg^{2+} and K^+ in the crystal dissolution by Spectroquant® test kit (Merck, Germany) and AAS. The data collected from the duplicates were analysed by using mean and standard deviation

3. Results and discussion

3.1 Microorganism growth and activity in synthetic media

The five microbial strains investigated were observed to grow in their synthetic solution (Fig. 1). The microbial growth displayed no lag phase and the growth rates (μ) were between 0.16 and 0.28 1/h, during the initial 24 h of incubation (exponential phase) (Fig. 1, Table S1). These growth rates were higher than those previously estimated (μ <0.05 1/h) using turbidity measurements (Soares et al., 2014). The *B. antiquum* growth rate observed in this study (μ=0.21 1/h) was the same order of magnitude than previously reported (maximum μ=0.14 1/h) in wastewater with presence of NaCl (3% w/v) and using acetate as the major carbon source (equivalent to 1124 mg chemical oxygen demand/L) (Simoes et al., 2017). The SCOD removal was 48–68% (initial value about 3500 mg/L) by the end of the incubation time (Table S1). Neither intact cell counts nor SCOD reduction was observed in non-inoculated controls (Table S1).

SP

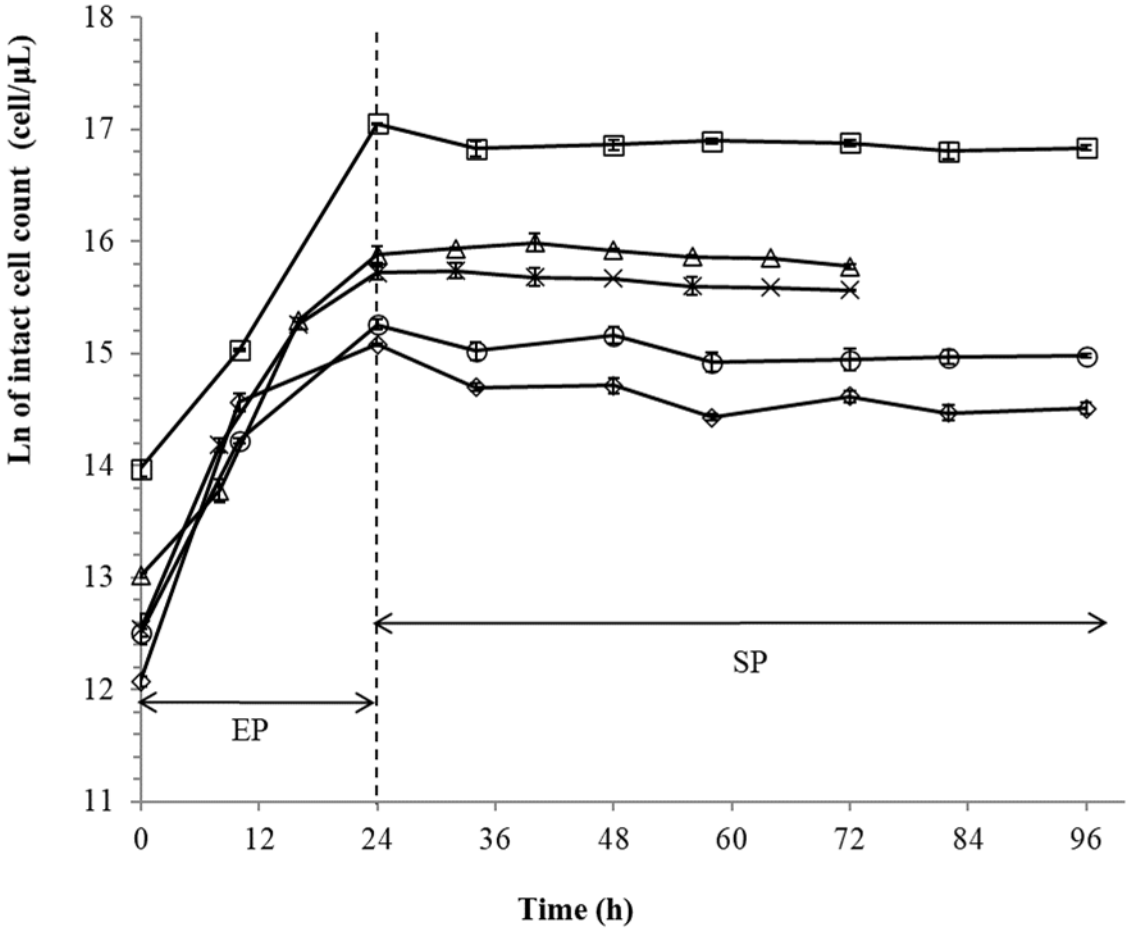


Fig. 1. Natural logarithm of intact cell count of *H. salinarum* (×), *B. antiquum* (Δ), *B. pumilus* (◊), *M. xanthus* (○) and *I. loihiensis* (□) over the incubation period. Error bars indicate standard deviation of duplicates. (EP - exponential phase, SP - stationary phase of growth)

The major carbon source in B41 media was yeast extract, that is rich in protein (50–75%) and carbohydrates (4–13%) (EURASYP, 2014). Protein was reported as the preferred carbon source for the selected microorganisms (Leng et al., 2020). After 24 h incubation, the media still contained significant amounts of SCOD and the cultures reached stationary phase of growth (Fig. 1). A concentrated yeast extract solution (10 g/L) of 10 mL was added to the *B. pumilus* culture during the stationary phase of growth (96 h). A concentrated yeast extract solution (10 g/L) of 10 mL was added to the *B. pumilus* culture during the stationary phase of

180 growth (96 h). In the subsequent 34 h incubation time, the intact cell count doubled. The
181 portion of PO_4-P (50%) and Mg^{2+} (100%) introduced by the concentrated yeast extract solution
182 was consumed, along with overall increases of pH (2%) and NH_4-N (3.8 fold). The microbial
183 growth influenced chemical characteristics of solution thus the crystallisation process. The
184 limitation in microbial growth might reduce the potential of nutrients removal and recovery by
185 crystallisation. Because yeast extract is a nutrient-rich complex, it not only serves as a carbon
186 source, but also provides B-complex vitamins, nitrogen, amino acids, carbon and trace minerals
187 (e.g. iron, selenium, zinc) necessary for microbial growth. A wide spectrum of microorganisms,
188 particularly bacteria, require B-complex vitamins as functional coenzymes for many oxidation-
189 reduction reactions that are involved in growth and energy transformation (Jurtshuk, 1996).
190 Due to the high dissolved oxygen (maintained at 6–8 mg/L) and the amount of organic carbon
191 source remaining (measured as SCOD after 24 h of incubation), when the stationary phase of
192 growth was reached, the limitation in microbial growth might have resulted from lack of
193 essential macro/micro nutrients. Furthermore, mass transfer coefficient to and from the cells
194 might have been limited once combined saturation of cells and crystals in the solution hindered
195 the transport of mass needed for cell growth and duplication.

196 Microbial cell clusters, during the exponential phase of growth, were frequently found around
197 (Fig. 2 a), or aggregated to the formed crystals (Fig. 2 e) in inoculated synthetic solution. A
198 process of small particles around 1 μm (Fig. 2 b) aggregating (Fig. 2 c) to form triangle or
199 trapezoidal crystals with crystalline structure (Fig. 2 d) was observed for all the five
200 investigated microbial cultures. The sizes of such small particles were the same order of
201 magnitude than those of the investigated microbial cells' (Leng et al., 2020). An evolution of
202 crystal morphology from cell cluster to bulk crystal with smooth surface was also observed
203 (Fig. 2 e–g). Crusted two-cell or tetrad clusters in *B. pumilus* culture (Fig. 2 h) occurred in the
204 early exponential phase of growth (10 h) and throughout the incubation period. Such structures
205 did not grow in sphere size but had the potential to aggregate together or onto the crystal surface
206 (Fig. 2 i). These specific cell structures observed in *B. pumilus* cultures were similar as
207 previously reported for mineralized embryo-infesting *Thiomargarita* cells (Bailey et al., 2007)
208 and silica spheroids attached onto the cell membrane in microbial silicification (Yee et al.,
209 2003). Thus, the crusted cell structures observed during *B. pumilus* growth in this study were
210 likely associated with the epicellular mineralisation, which is referred as BIM process (Mann,
211 2001). The cell outer layer of both Gram-positive and Gram-negative bacteria are

predominantly negatively charged, which enables the interaction and accumulation of cations onto the surface for mineral precipitation (Frankel and Bazylinski, 2003; Orange et al., 2009).

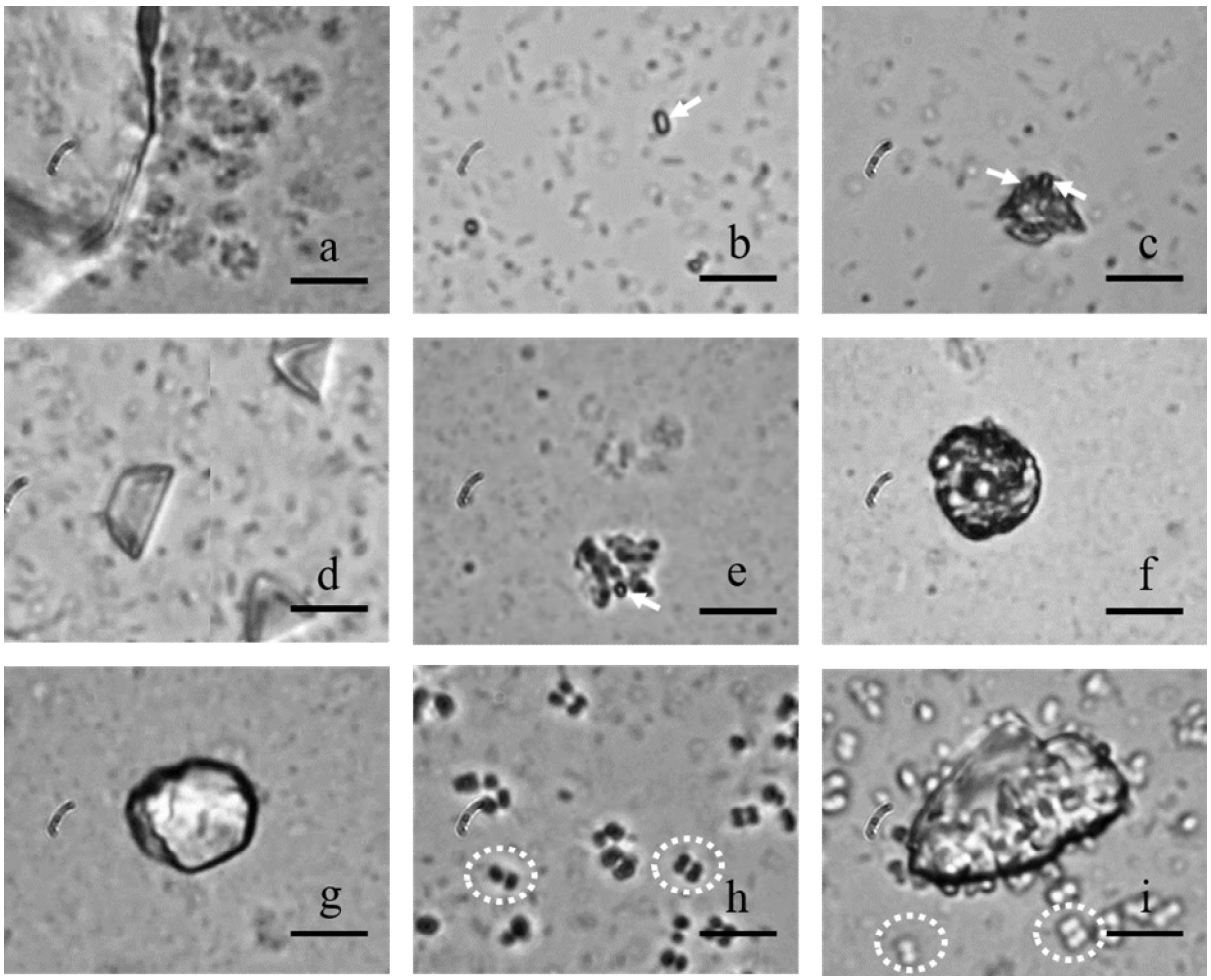


Fig. 2 Optical microscope photograph observed in late exponential phase of growth (16–24 h): (a) cell clusters of *I. loihiensis* around crystal surface, (b) small particles (white arrow) about 1 µm in *M. xanthus* culture, (c) aggregate of small particles (white arrows) in *B. antiquum* culture, (d) triangle and trapezoidal crystals in *M. xanthus* culture, (e-g) a morphology evolution in *I. loihiensis* culture: from (e) aggregate of cell clusters and particles (white arrow) to (f) large particle (approx. 5 µm) with clear boundary, and to (g) large particle (approx. 5 µm) of crystalline structure view. (h) Crusted two-cell or tetrad cell clusters in *B. pumilus* culture, and (i) their aggregate onto crystal surface (white dotted circle - crusted cell cluster). Bar scale - 4.06 µm.

Gram-positive microorganisms have been reported to have more potential to form a thick mineral crust around the cell due to their thick outer layer of peptidoglycan (Westall, 1999). Furthermore, extracellular polymeric substances (EPS) such as the secreted carboxylate groups or phosphate groups may bond into the peptidoglycan framework within the Gram-positive cell envelope to increase the electronegative charge density, and thus resulting in highly interactive cations (Schultze-Lam et al., 1996). It is suggested that *B. pumilus* can form mineral nuclei along the cell surface during rapid growth in solutions rich in PO_4-P and Mg^{2+}, and the nucleus can firmly attach to the cell surface to completely encrust the cell minerals.

3.2 Crystal identification and morphology

All tested microorganisms produced crystals in solution, and no crystal was observed in the non-inoculated controls. The diffraction results showed that the peak profiles of the isolated purified crystals' X-ray powder diffractometer (XRD) curves met that of the standard curve, with preferentially oriented directions of [011], [00$\bar{1}$] and [111] (Fig. S1), the same as those of abiotic struvite (Table S2). Hence, it can be concluded that the crystals recovered from the solutions inoculated with the microorganisms were struvite. However, the bio-struvite diffraction peaks varied slightly between microbial strains and thus different crystal morphology was observed. The bio-struvite crystal morphology was mainly a thin trapezoidal platy shape (*H. salinarum, B. pumilus* and *M. xanthus*) (Fig. S2 a–c), coffin-lid shape (*B. antiquum*) (Fig. S2 d) and long-bar shape (*I. loihiensis*) (Fig. S2 e). In particular, the morphology of coffin-lid shaped bio-struvite crystal resulted from large [00$\bar{1}$] faces as the bottom and small [001] faces as the top (Fig. S1), and crystals with truncated apices was observed in *B. antiquum* culture (Fig. S2 d), indicating a loss of rectangular symmetry. These observed three morphologies were among the typical forms of struvite (Tansel et al., 2018), but were different from that of the abiotic struvite precipitated in this study (pH 9, $SI_{struvite} > 4$), typically small and with a dendritic structure (Fig. S2 f). There was no evidence showing a possibility of trapezoidal-platy shaped and coffin-lid shaped bio-struvite crystals produced by dendritic abiotic struvite crystal. Because the dendritic morphology with high aspect ratios resulted from relative high pH (e.g. pH ≥9.5) and supersaturation (e.g. $SI_{struvite}$ ≥7.9) in comparison to the pH and supersaturation level required for the formation of the other two morphologies (Shaddel et al., 2019). The self-assembly of crystals by contact twining on [001] (Fig. S2 g) and [00$\bar{1}$] unite (Fig. S2 h) or parallel growth (Fig. S2 i) was also observed in this

study. The contact twining on [001] and [00$\bar{1}$] unite was reported among the most typical twinning types of struvite (Mindat, 2018). Particularly, the contact twining of coffin-lid and long-bar shaped bio-struvite along the [00$\bar{1}$] direction (Fig. S2 g) observed in this study may be associated with a trend to form homogeneous morphology via Ostwald ripening to fill the gap space and to smoothen the surface (Ratke and Voorhees, 2013).

Microorganisms have been reported to influence the crystal morphology by secreting/functioning specific substances such as polysaccharides and lipopolysaccharides with anionic nature, which are responsible for the selective interaction with the molecular structure of the crystal surface (Prywer et al., 2012). Such interactions have been reported to slow down the growth of specific crystal faces, and therefore change the crystal morphology (Sadowski et al., 2014). In the case of coffin-lid like bio-struvite in *P. mirabilis* cultures, cells' selective binding to the [00$\bar{1}$] faces with high density Mg^{2+} octahedral, other than [001] faces terminated by NH_4^+ tetrahedral, resulted in slowed down growth of [00$\bar{1}$] and enhanced the face expression, whereas the [001] face grow freely and consequently are smaller than the [00$\bar{1}$] face (Prywer et al., 2012). Thus, the microorganisms investigated in this study are suggested to be capable of synthesising specific organic molecules that have preference to bind to [00$\bar{1}$], [111] and especially [011] faces of bio-struvite crystals, influencing the morphology.

The characterization of bio-struvite was further identified in a comparison with abiotic struvite prepared in this study by a standard chemical way. Similar stoichiometric ratios of the component elements (based on weight percent, wt %) of the bio-struvite and abiotic struvite were obtained: the molar ratio of [Mg]:[P]:[O]:[N] of the crystal surface structure was approx. 1.0:1.0:8.8:0.2, and the [Mg^{2+}]:[PO_4-P]:[NH_4-N] in crystal dissolution was 1.0:1.0:1.0 (Table S3). Therefore, the crystals produced by the selected microorganisms were similar to the abiotic struvite standard. An observed loss of nitrogen and oxygen in the composition of the struvite and bio-struvite analysed was due to the crystal air-drying method that caused volatilization of ammonia and water molecules within the crystalline frameworks, especially on the crystal surface, as previously described (Bhuiyan et al., 2008a).

Potassium was only found in the bio-struvite: 1.3–2.5 wt % on the crystal surface and 1.1–1.8 wt % in the crystal dissolution (Table S3). As an essential macronutrient required for microbial growth, K accounts for 1% of microbial cells on a DW basis (Stolp, 1988) and has potential to

participate into electrostatic interaction between charged residues on the cell outer layer and crystal surface (Sadowski et al., 2014). In this study, it is suggested that through electrostatic interaction, the microbial cells can bond to the crystal surface and help settle additional K^+ onto the surface.

3.3 Bio-struvite production and uptake of nutrients

The microorganisms produced about 1500 mg bio-struvite crystals (≥10 μm) per litter of solution, corresponding to an approx. recovery of 190 mg/L PO_4-P and 150 mg/L Mg^{2+}, of the nutrients in solution (Table 1). The formation of bio-struvite resulted in the removal of PO_4-P and Mg^{2+} from the B41 media by the end of the incubation period (Table 1). The most significant reduction of PO_4-P and Mg^{2+} occurred during the microbial exponential phase (0–24 h), with removal of 37–50% and 58–74%, respectively (Fig. 3 a–b). It is noted that *B. antiquum* removed up to 71% of PO_4-P and 99% of Mg^{2+} by the end of 72 h incubation (Table 1). Yet only 50% of the PO_4-P and 87% of Mg^{2+} was recovered by bio-struvite (≥10 μm) (Table 1). Similarly, in *I. loihiensis* cultures, around 65% PO_4-P and 95% Mg^{2+} was removed from solution but only 46% PO_4-P and 73% Mg^{2+} was recovered as bio-struvite (≥10 μm) (Table 1). Besides the loss potential of small bio-struvite crystals (<10 μm) during filtration, the data obtained suggests accumulation of PO_4-P and Mg^{2+} within cytoplasm or cell structures, as reported in *P. tetraurelia* cells (Grover et al., 1997) and in *B. antiquum* (Simoes et al., 2017; Smirnov et al., 2005). Furthermore, the presence of Mg^{2+} has been reported to be vital for biological PO_4-P removal as bio-struvite (Smirnov et al., 2005). In this study, the lack of Mg^{2+} at the end of incubation may limit the bio-struvite production and PO_4-P removal that could be further promoted by adding more Mg^{2+} sources.

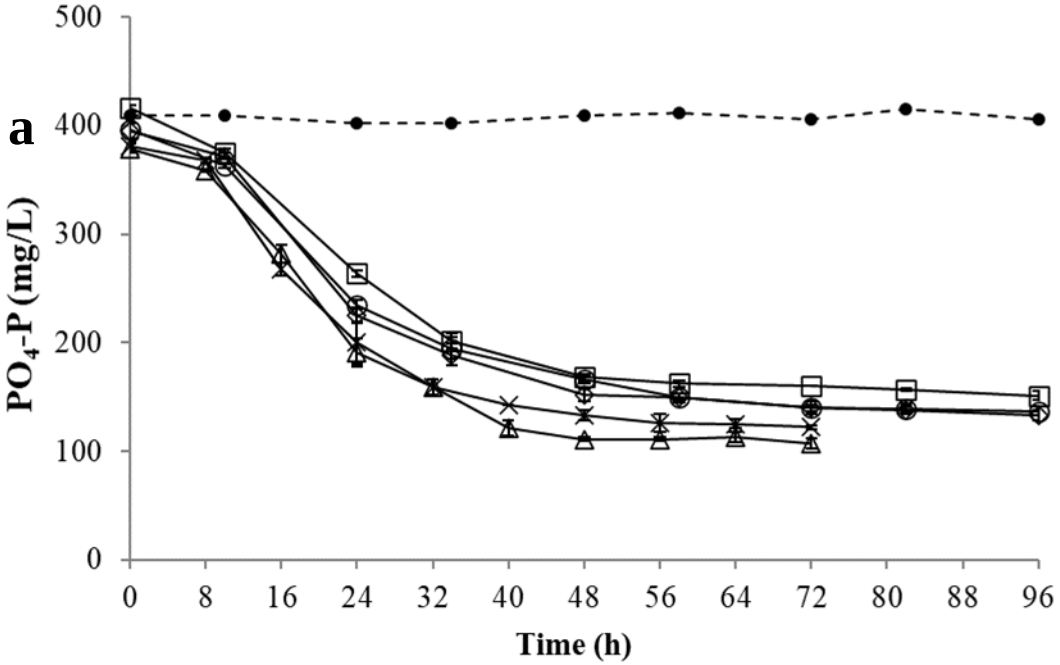
Overall, the concentrations of NH_4-N and pH of the solution increased by the end of the incubation period (Table 1). A rapid increase of NH_4-N was observed within the first 24 h of incubation (Fig. 3 c), corresponding to the rapid microbial growth in the exponential phase (Fig. 1). Slight pH drop (≤0.3 units) was observed in the early exponential phase (0–10 h), which may result from accumulation of carbon dioxide in the solution. Such a pH reduction was followed by a steady increase until the end of the incubation period (Fig. 3 d). The *B. antiquum* and *I. loihiensis* were observed increasing overall pH by 1.0 units, which was higher than for the other three microorganisms (by 0.7–0.9 units), corresponding to the NH_4-N production (Table 1). The synthesis of bio-struvite, especially through BIM process, has been

reported to be related to the microbial capability to biodegrade N-rich compounds in culture media to release NH_4-N and raise pH (Sinha et al., 2014). The microbial growth hence created a mild alkaline environment where the Mg^{2+} was no longer soluble and integrated with PO_4-P and NH_4-N to precipitate as bio-struvite (Smirnov et al., 2005). The microorganisms investigated in this study were known to be capable of using proteins/amino acids as a carbon source (Leng et al., 2020). Thus, the yeast extract applied in this study was not only providing microbial growth with a carbon source but also was used as the main source for NH_4-N production.

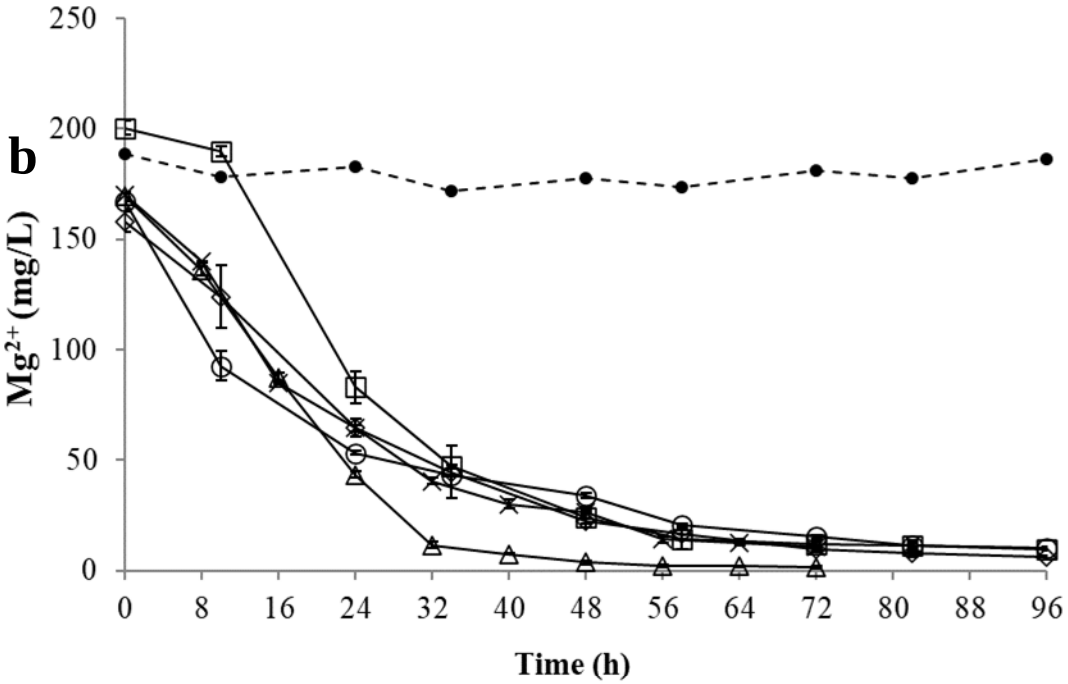
Table 1 Bio-struvite production (mg bio-struvite per litter of solution), changes of pH, PO_4-P, NH_4-N and Mg^{2+} and in the presence of microbial strains by the end of 72 h (*H. salinarum* and *B. antiquum*) and 96 h (*B. pumilus*, *M. xanthus* and *I. loihiensis*) incubation and in non-inoculated control (average ± standard deviation of duplicates).

	H. salinarum	*B. antiquum*	*M. xanthus*	*B. pumilus*	*I. loihiensis*	Control
Bio-struvite production[1]	1567 ± 41 mg/L	1509 ± 55 mg/L	1536 ± 110 mg/L	1515 ± 72 mg/L	1481 ± 39 mg/L	0 mg/L
pH increase	0.7 ± 0.0	1.0 ± 0.0	0.8 ± 0.1	0.8 ± 0.0	1.0 ± 0.0	< 0.1
NH_4-N increase	71 ± 6 mg/L	105 ± 6 mg/L	71 ± 8 mg/L	69 ± 5 mg/L	105 ± 4 mg/L	< 1 mg/L
PO_4-P removal	259 ± 6 mg/L 68%	273 ± 8 mg/L 71%	239 ± 17 mg/L 63%	256 ± 11 mg/L 65%	279 ± 7 mg/L 67%	< 1 mg/L 0%
Mg removal	159 ± 2 mg/L 94%	168 ± 3 mg/L 99%	157 ± 5 mg/L 94%	152 ± 5 mg/L 96%	191 ± 3 mg/L 95%	< 1 mg/L 0%
PO_4-P recovered as bio-struvite crystals[1]	192 mg/L 50%	191 mg/L 50%	192 mg/L 51%	191 mg/L 48%	190 mg/L 46%	0 0%
Mg^{2+} recovered as bio-struvite crystals[1]	149 mg/L 88%	148 mg/L 87%	149 mg/L 89%	148 mg/L 93%	147 mg/L 73%	0 0%

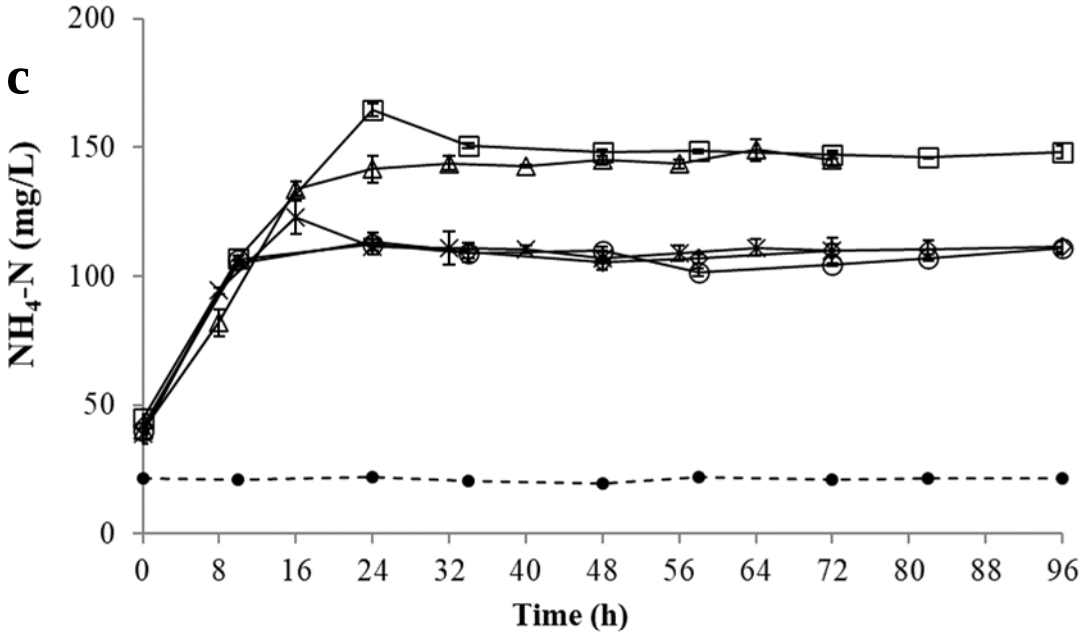
[1] - Bio-struvite crystals ≥10 μm


a
500
400
300
200
100
0
PO4-P (mg/L)
0
8
16
24
32
40
48
56
64
72
80
88
96
Time (h)

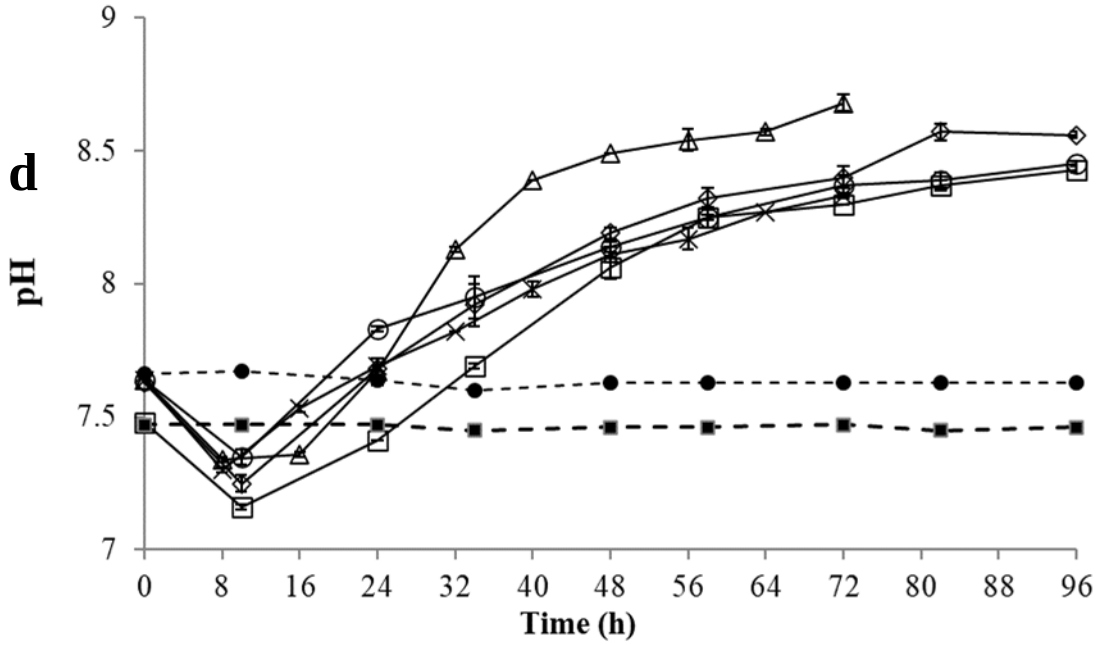
329


b
250
200
150
100
50
0
Mg2+ (mg/L)
0
8
16
24
32
40
48
56
64
72
80
88
96
Time (h)

330



331



332

333 **Fig. 3 Variation of (a) PO_4-P, (b) Mg^{2+}, (c) NH_4-N and (d) pH in microbial cultures of *H.***
334 ***salinarum* (×), *B. antiquum* (Δ), *B. pumilus* (◊), *M. xanthus* (○) and *I. loihiensis* (□) and in**
335 **non-inoculated controls (●) and (■) during 72/96 h incubation time. Error bars indicate**
336 **standard deviation of duplicates.**

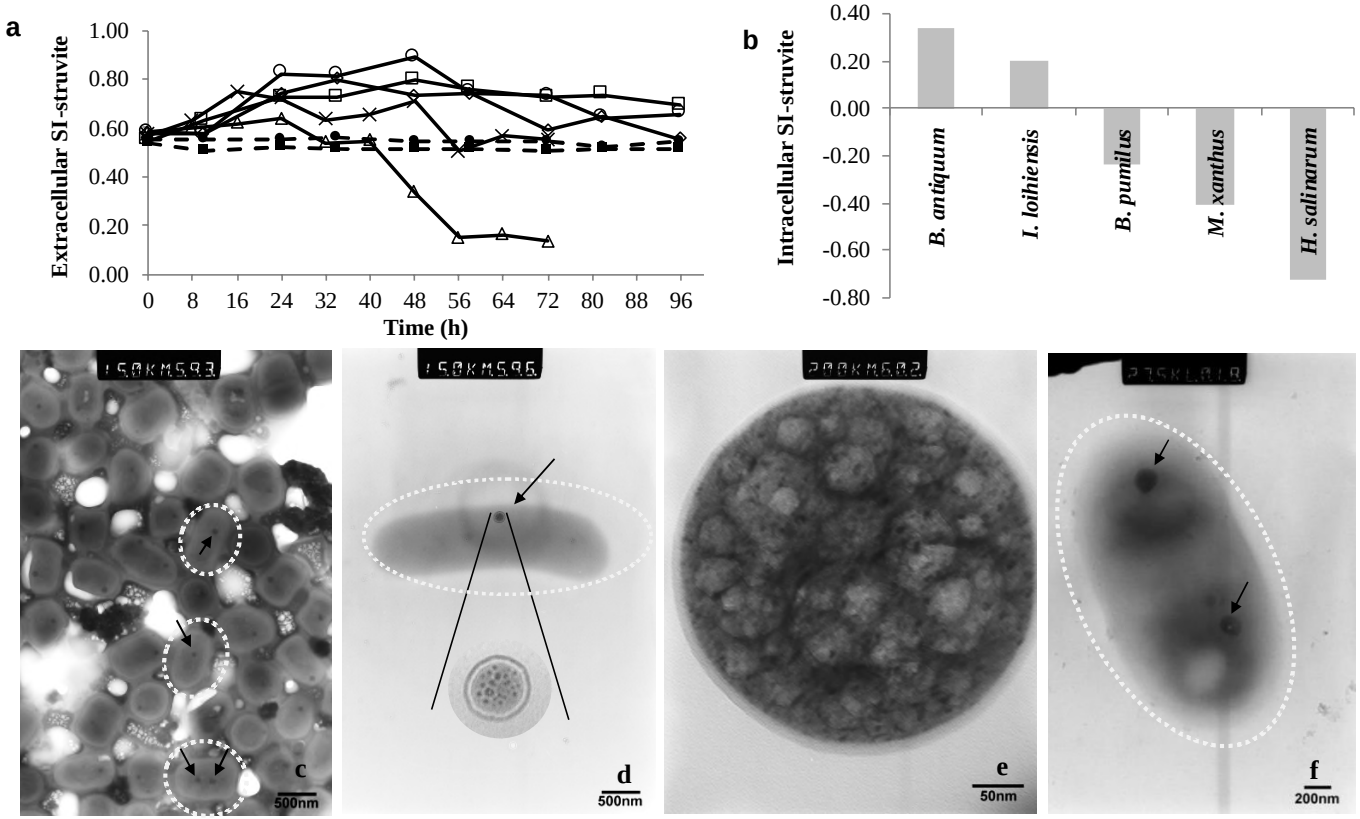
3.4 Extracellular and intracellular supersaturation

In the presence of microorganisms, the extracellular (or solution) supersaturation index of struvite ($SI_{struvite}$) in synthetic solutions increased from an initial value of around 0.57 to values between 0.64 (*B. antiquum*, 24 h) and 0.89 (*M. xanthu*s, 48 h) within the 48 h incubation time (Fig. 4 a). The $SI_{struvite}$ of inoculated solution then steadily dropped to values between 0.13 (*B. antiquum*, 72 h) and 0.69 (*I. loihiensis*, 96 h) by the end of the incubation time, while the solution $SI_{struvite}$ of the control was maintained at a constant level (0.51–0.56) (Fig. 4 a). In particular, the bio-struvite crystals were observed during the microbial exponential phase (8–24 h) (Fig. 1) when solution $SI_{struvite}$ achieved 0.6–0.8 (Fig. 4 a).

When comparing the solution $SI_{struvite}$ curve with those of pH and concentrations of NH_4-N, PO_4-P and Mg^{2+}, the extracellular $SI_{struvite}$ (except that of *B. antiquum* culture) was observed with relatively slight changes with time. It is suggested that the release of NH_4-N and pH increase played a key role in maintaining the solution $SI_{struvite}$ for the crystallization process until the end of the incubation even when the concentration of Mg^{2+} (3–30 mg/L) limited the solution $SI_{struvite}$ after 48 h incubation time. Solution $SI_{struvite}$ has been recognized as the driving force for the crystallization process (De Yoreo et al., 2015). When comparing the solution $SI_{struvite}$ eligible for bio-struvite formation ($SI_{struvite}$ =0.6–0.8) in this study with those previously reported for abiotic struvite formation, for example a minimum $SI_{struvite}$ of 1.2 (Galbraith and Schneider, 2009) and technique scale-based optimal $SI_{struvite}$ between 2–6 (Bhuiyan et al., 2008b), the bio-struvite can nucleate in solution with relatively low $SI_{struvite}$ where the nucleation of abiotic struvite may not occur without seeding. The different supersaturation levels required for nucleation suggested a way to differentiate bio-struvite mineralisation from abiotic struvite precipitation. This is related to another significant role microorganisms play in biomineralisation: negatively charged specific organic structures (e.g. peptidoglycan layer) or substances secreted by organisms (e.g. EPS) may serve as heterogeneous nucleation sites by interacting/accumulating cations and entrapping crystal seeds for precipitation (Arias et al., 2017; Decho, 2000). The cell surface layer was recognized as the main crystalline bio-structure that can act as a nucleus (Braissant et al., 2003). In particular, González-Muñoz et al. (2010) reported the importance of the presence of *M. xanthu*s cells in the crystallization of bio-struvite, irrespective of whether the cells were living or dead (entire or disrupted).

The intracellular $SI_{struvite}$ of the studied microorganisms indicated their potential to form intracellular bio-struvite crystals (Fig. 4 b). *B. antiquum* and *I. loihiensis* were observed to have an intracellular $SI_{struvite}$ >0 (Fig. 4 b). This is in agreement with previous observations that *B. antiquum* and *I. loihiensis* might uptake and accumulate a considerable amount of PO_4-P and Mg^{2+} within their cells (Table 1). These accumulated nutrients might combine with NH_4-N inside cells, for intracellular bio-struvite formation. Furthermore, transmission electron microscopy (TEM) images showed that most *B. antiquum* cells contained several membrane-bound intracellular compartments enclosing electron dense clustered granules (Fig. 4 c–e). These cell structures are suggested to be lipid vesicles, due to a similar structure to previously reported lipid vesicles (Spiegel et al., 2013). Similar intact membrane-bound structures enclosing electron dense clustered materials were observed inside *I. loihiensis* cell (Fig. 4 f).

Although a high-energy electron beam was reported to destroy small/thin granules (Omar et al., 1998), and thus the occurrence of dispersive clustered materials (Fig. 4 e), such intact membrane-bound compartments occupied with electron dense granules/materials suggested that intracellular vesicles were where crystallization took place. This was supported by several studies because water-insoluble phosphates were observed in the cytoplasm of *B. antiquum* cells that were grown in medium rich in P and Mg^{2+} (Smirnov et al., 2005).



384

385 **Fig. 4 Variation of extracellular $SI_{struvite}$ (a) in microbial cultures of *H. salinarum* (×), *B. pumilus* (◊), *M. xanthus* (○), *B. antiquum* (Δ) and**
386 ***I. loihiensis* (□), and the microbial intracellular $SI_{struvite}$ (b) during the 72/96 h incubation time. TEM pictures shows (c) an overview of *B.***
387 ***antiquum* culture (60 h), cells (white dotted circles) containing one or two electron-dense structures (black arrows); (d) a vesicle-like**
388 **structure (black arrow) inside *B. antiquum* cell (white dotted circles), with intact membrane structure, and occupied with electron dense**
389 **clustered granules, as shown in an enlarged (8-time) version; (e) detail of the vesicle, whose internal structures were destroyed by a high-**

energy electron beam, resulting in the internal space being full of dispersive clustered materials and bubbles; (f) electron-dense clustered materials (black arrows) inside *I. loihiensis* cell (white dotted circles) after 60 h incubation period.

Others have reported the occurrence of morphologically homogenous struvite in the *P. tetraurelia* cell cytoplasm (Grover et al., 1997), and the formation of minerals enclosed by multi-layered ultrastructure within cells' cytoplasm (Bailey et al., 2007). Thus, the bio-struvite mineralisation by *B. antiquum* and *I. loihiensis* cultures was suggested as a BCM process, where the bio-struvite is produced in intracellular functional structures (Grover et al., 1997). Yet it is not known whether its ability to produce intracellular phosphates minerals in nutrient-rich conditions can help them survive in stress or nutrient-poor conditions. No similar cell structure was seen in the other three microbial cultures during their stationary phase.

3.5 Bio-struvite crystal growth

A rapid crystal growth occurred during the microbial exponential phase of growth (8–24 h), when D_{v50}, the particle median diameter for a volume distribution, increased from 0 to 85–145 μm, and the percentage of crystals above 100 μm increased from 0 to 44–71% (Fig. 5). The rapid growth was followed by a constant level of size distribution that was maintained until the end of the incubation period, when large crystals above 100 μm finally represented 55–87% of total particles (Fig. 5). No crystal was observed in the control (Fig. 5).

The crystal growth was correlated to the variation of solution $SI_{struvite}$ (Fig. 4 a), where the rapid increase of values occurred after 8–24 h incubation time, reached peak values within 48 h and maintained $SI_{struvite} > 0$ until the end of the incubation period. In particular, the crystal growth in *B. antiquum* culture was maintained at a constant level ($D_{v50} \approx 100$ μm) after 40 h incubation, even with a reduction of solution $SI_{struvite}$ from 0.55 to 0.13 in *B. antiquum* culture (Fig. 4 a).

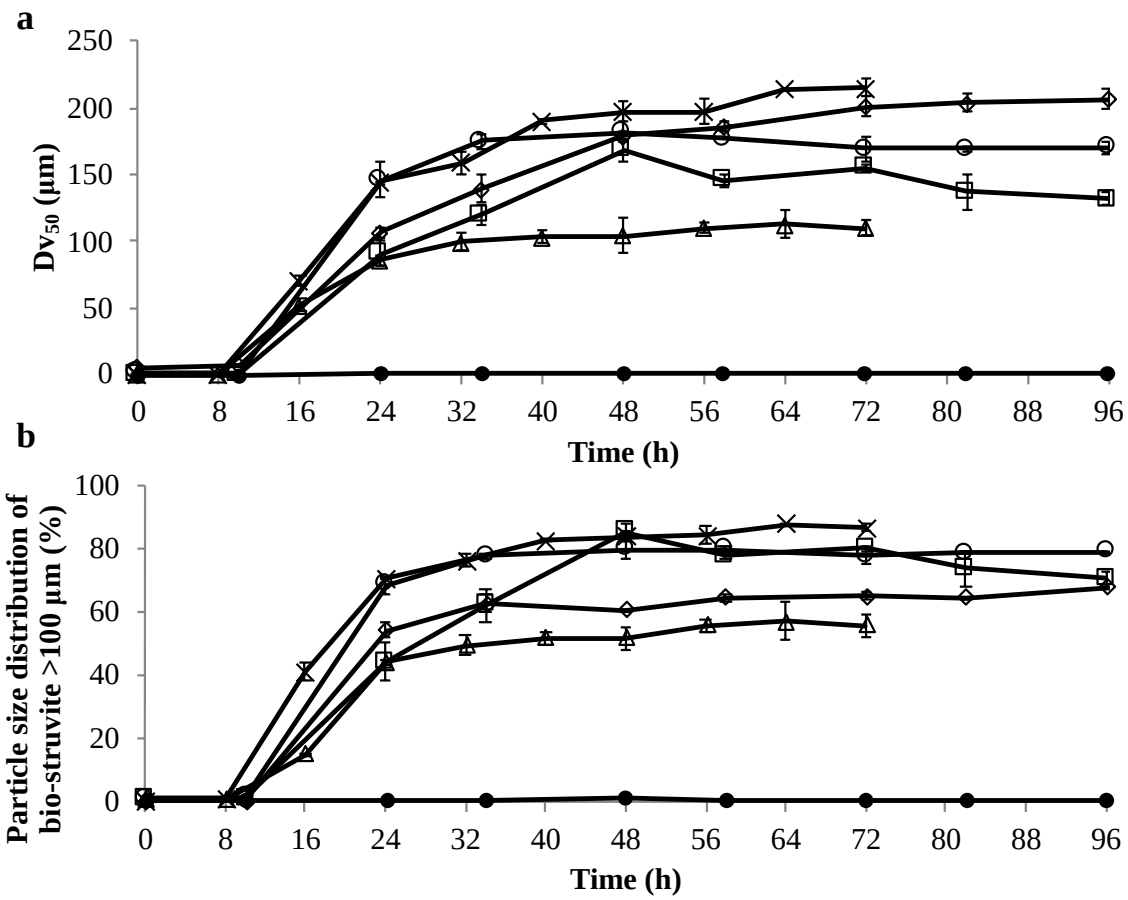


Fig. 5 Variation of D_{v50} (a) and cumulative volume percentage of crystal ≥ 100 µm (b) in synthetic solution over incubation period, in the presence of *H. salinarum* (×), *B. antiquum* (Δ), *B. pumilus* (◊), *M. xanthus* (○) and *I. loihiensis* (□) and in non-inoculated controls (●). Error bars indicate standard deviation of duplicates. D_{v50} is the value of particle diameter at 50% in the cumulative particle size distribution on a volume basis.

Based on the final crystal size distribution (Fig. 5), the microorganisms could be identified into two groups: *H. salinarum, B. pumilus* and *M. xanthus* produced large crystal groups (Dv_{50} =170–215 µm), with a gap size between Dv_{50} and Dv_{90} (i.e. Dv_{90} - Dv_{50}) of a wide range about 200 µm; *B. antiquum* and *I. loihiensis* produced relatively small crystal groups (Dv_{50} =110–130 µm), with narrow gap range (Dv_{90} - Dv_{50}) about 110 µm (Table S4). Such crystals within a narrow size range of distribution suggest homogeneous size and better reproducibility (Fig. S3), which can be correlated to the BCM process, where the biomineral products are highly biologically controlled (Sinha et al., 2014).

3.6 Bio-struvite biomineralisation mechanisms

The analysis of microbial growth and activities, crystal growth and morphology, $SI_{struvite}$ and TEM observations supports the distinction of BCM from the BIM process amongst the microorganisms investigated: *B. antiquum and I. loihiensis* could produce bio-struvite in synthetic solution via BCM process, whereas *H. salinarum, B. pumilus and M. xanthus* produce bio-struvite through BIM process (Table 2). In both processes the microorganisms biodegraded proteins to create supersaturated conditions for bio-struvite mineralisation. The presence of cells/cell clusters was reported to reduce the energy barrier and $SI_{struvite}$ for heterogeneous nucleation (Arias et al., 2017; Decho, 2000), and also exerted influence on the crystal morphology. BIM occurs in open environments under poor cellular control where the composition of the solution highly influences biomineralisation and therefore the crystals produced in this study were heterogeneous in size and morphology, which was similar to their chemical counterparts. In contrast, isolated environment such as lipid vesicles ensure BCM specific conditions where the chemical composition of solution and location of bio-struvite was highly cellular controlled, and therefore the biomineral product was observed of higher reproducibility and homogeneity. For example, the bio-struvite production by *B. antiquum* was also observed in a different synthetic media, whereas *H. salinarum* did not produce struvite in this media, but induced $Mg_2PO_4OH{\bullet}4H_2O$ crystals instead (Smirnov et al., 2005).

Table 2 Key features of bio-struvite mineralisation by *H. salinarum, B. antiquum, B. pumilus, M. xanthus and I. loihiensis* in synthetic B41 solution.

	Biologically induced mineralisation	Biologically controlled mineralisation
H. salinarum	• pH elevation • NH_4-N production • Crystal morphology heterogeneity • Crystal heterogeneous size: Dv_{90}–Dv_{50} =189.00 μm • Intracellular $SI_{struvite}$ = -0.72	
B. antiquum		• pH elevation • NH_4-N production • Crystal morphology homogeneity • Crystal size homogeneity: Dv_{90}–Dv_{50} =103.00 μm • Clustered materials enclosed in intracellular membrane-bound structures • Intracellular $SI_{struvite}$ = 0.34
B. pumilus	• pH elevation • NH_4-N production • Crystal morphology heterogeneity • Crusted cell/cell clusters • Crystal heterogeneous size: Dv_{90}–Dv_{50} = 284 μm • Intracellular $SI_{struvite}$ = -0.24	
I. loihiensis		• pH elevation • NH_4-N production • Crystal morphology homogeneity

		• Crystal size homogeneity: Dv_{90}–Dv_{50} =113 μm • Clustered materials enclosed in intracellular membrane-bound structures • Intracellular $SI_{struvite}$ = 0.20
M. xanthus	• pH elevation • NH_4-N production • Crystal morphology heterogeneity • Crystal heterogeneous size: Dv_{90}–Dv_{50} =179 μm • Intracellular $SI_{struvite}$ = -0.40	

3.7 Application of BCM for nutrient recovery by bio-struvite from municipal wastewater treatment

The total P in municipal wastewater typically varies between 5 and 20 mg/L, of which 1–5 mg/L is organic P and the rest is inorganic P (Ivanov et al., 2005). Both inorganic and organic P resources were reported to have potential use for bio-struvite production (Simoes, 2017). Wastewater also contains NH_4-N and biological degradable nitrogenous material which is essential for bio-struvite production. Moreover, WWTP location (hard water area, coastal area and receiving industrial discharge) and applied process (e.g. clay material used as supports in anaerobic digester release and ion exchange) can contribute to Mg^{2+} source (Jardin and Pöpel, 2001).

Despite the rich storage of these three nutrients in WWTP, the P recovery by abiotic struvite precipitation still requires an additional chemical dose/applied process (e.g. ion exchange) to adjust the pH and increase the PO_4-P (Mijangos et al., 2004), as well as seeding that is widely applied to reduce the energy barrier for crystallization (Doyle and Parsons, 2002), hence adding costs. This study reveals the microbial capability of the selected microorganisms to increase the potential of bio-struvite production in waste streams with low PO_4-P and low $SI_{struvite}$. That is, the application of bio-struvite can reduce the expense for the pH adjustment and PO_4-P elevation. However, real wastewater is a multi-phase fluid with lots of materials in different

chemical and physical states. Thus, actual mass transfer coefficients may be affected because of all of these substances. Furthermore, although both BIM and BCM are capable of removing N and P from wastewater by bio-struvite, BIM cannot provide crystals products of stable physiochemical characterization (Mann, 2001). Because such a biomineralisation process is sensitive to the environment and can be significantly influenced by the extreme complexity of wastewater, this may result in other kinds of phosphate minerals. BCM, however, formed in compartmentalized microenvironments and was highly regulated by cells. This study also proposed two bacteria (*B. antiquum* and *I. loihiensis*) involved in BCM bio-struvite formation, which have potential to recover nutrients such as N and P from wastewater by bio-struvite of more controlled quality. Increasing the difficulty of keeping *B. antiquum* and *I. loihiensis* as pure culture in real wastewater with inherent microbial communities, application of appropriate processes and optimisation of operational parameters (e.g., temperature, pH, carbon source) will allow preferential growth conditions for the desired bacteria to out-compete other microorganisms in complex microbial population.

4. Conclusions

- The microorganisms investigated can biodegrade proteins to release NH_4-N and raise the pH to create supersaturated condition for bio-struvite to nucleate. The presence of microbial cells reduced the $SI_{struvite}$ for bio-struvite heterogeneous nucleation, which enables bio-struvite to be produced at low PO_4-P.
- The investigated microorganisms predominantly produced bio-struvite crystals of either coffin-lid, long-bar or trapezoidal-platy shapes and they exerted influence on the crystal morphology.
- The occurrence of crusted cell/cell clusters in *B. pumilus* culture is related to epicellular mineralisation. *H. salinarum*, *B. pumilus* and *M. xanthus* produced bio-struvite of heterogeneous size through the BIM process, as a result of poor cellular control during the biomineralisation.
- *B. antiquum* and *I. loihiensis* produced bio-struvite through the BCM process, of homogeneous size and morphology and better reproducibility, as a result of high cellular control during biomineralisation. The intracellular $SI_{struvite}$ was high, where membrane-bound compartments occupied with electron-dense granules/materials were observed in the cytoplasm. *B. antiquum* and I. *loihiensis* are proposed to have potential to recover nutrients

from waste streams by bio-struvite of more controlled quality. Such potential and capability of all the selected microbial strains to produce bio-struvite in real municipal wastewater, will be investigated for the wastewater impact on mechanisms involved in biomineralization process.

References

Ali, M.I., Schneider, P. a., Hudson, N., 2005. Thermodynamics and solution chemistry of struvite. J. Indian Inst. Sci. 85, 141–149.

Arias, D., Cisternas, L., Rivas, M., 2017. Biomineralization mediated by ureolytic bacteria applied to water treatment: a review. Crystals 7, 345. https://doi.org/10.3390/cryst7110345

Bailey, J. V., Joye, S.B., Kalanetra, K.M., Flood, B.E., Corsetti, F.A., 2007. Evidence of giant sulphur bacteria in Neoproterozoic phosphorites. Nature 445, 198–201. https://doi.org/10.1038/nature05457

Bhuiyan, M.I.., Mavinic, D.., Koch, F.., 2008a. Thermal decomposition of struvite and its phase transition. Chemosphere 70, 1347–1356. https://doi.org/10.1016/j.chemosphere.2007.09.056

Bhuiyan, M.I.., Mavinic, D.., Koch, F.., 2008b. Phosphorus recovery from wastewater through struvite formation in fluidized bed reactors: A sustainable approach. Water Sci. Technol. 57, 175–181. https://doi.org/10.2166/wst.2008.002

Braissant, O., Cailleau, G., Dupraz, C., Verrecchia, E.P., 2003. Bacterially induced mineralization of calcium carbonate in terrestrial environments: the role of exopolysaccharides and amino acids. J. Sediment. Res. 73, 485–490. https://doi.org/10.1306/111302730485

Da Silva, S., Bernet, N., Delgenès, J.P., Moletta, R., 2000. Effect of culture conditions on the formation of struvite by Myxococcus xanthus. Chemosphere 40, 1289–1296. https://doi.org/10.1016/S0045-6535(99)00224-6

De Yoreo, J.J., Gilbert, P.U.P.A., Sommerdijk, N.A.J.M., Penn, R.L., Whitelam, S., Joester, D., Zhang, H., Rimer, J.D., Navrotsky, A., Banfield, J.F., Wallace, A.F., Michel, F.M., Meldrum, F.C., Cölfen, H., Dove, P.M., 2015. Crystallization by particle attachment in synthetic, biogenic, and geologic environments. Science (80-.). 349, aaa6760. https://doi.org/10.1126/science.aaa6760

Decho, A.W., 2000. Microbial biofilms in intertidal systems: an overview. Cont. Shelf Res. 20, 1257–1273. https://doi.org/10.1016/S0278-4343(00)00022-4

530 Doyle, J.D., Parsons, S. a., 2002. Struvite formation, control and recovery. Water Res. 36,
531 3925–3940. https://doi.org/10.1016/S0043-1354(02)00126-4

532 EURASYP, 2014. Natural yeast – the nutritious basis for yeast extract [WWW Document].
533 URL http://www.yeastextract.info/news-and-downloads/news/135/natural-yeast-the-
534 nutritious-basis-for-yeast-extract (accessed 2.1.20).

535 Frankel, R.B., Bazylinski, D.A., 2003. Biologically induced mineralization by bacteria, in:
536 Reviews in Mineralogy and Geochemistry. pp. 95–114. https://doi.org/10.2113/0540095

537 Galbraith, S.C., Schneider, P.., 2009. A review of struvite nucleation studies, in: International
538 Conference on Nutrient Recovery from Wastewater Streams. IWA publishing, London,
539 UK, pp. 69–78.

540 Gao, G., 2008. Physiological and ecological characteristics of blue-Green algae in Lake Taihu,
541 in: Qin, B. (Ed.), Lake Taihu, China: Dynamics and Environmental Change. Springer
542 Science & Business Media., pp. 197–227.

543 González-Muñoz, M.T., De Linares, C., Martínez-Ruiz, F., Morcillo, F., Martín-Ramos, D.,
544 Arias, J.M., 2008. Ca-Mg kutnahorite and struvite production by Idiomarina strains at
545 modern seawater salinities. Chemosphere 72, 465–472.
546 https://doi.org/10.1016/j.chemosphere.2008.02.010

547 González-Muñoz, M.T., Rodriguez-Navarro, C., Martinez-Ruiz, F., Arias, J.M., Merroun,
548 M.L., Rodriguez-Gallego, M., 2010. Bacterial biomineralization: new insights from
549 Myxococcus-induced mineral precipitation. Geol. Soc. London, Spec. Publ. 336, 31–50.
550 https://doi.org/10.1144/SP336.3

551 Grover, J.E., Rope, a F., Kaneshiro, E.S., 1997. The occurrence of biogenic calcian struvite,
552 (Mg,Ca)NH4PO4.6H2O, as intracellular crystals in Paramecium. J. Eukaryot. Microbiol.
553 44, 366–373.

554 Gustafsson, J.P., 2000. Visual MINTEQ.

555 Ivanov, V., Stabnikov, V., Zhuang, W.Q., Tay, J.H., Tay, S.T.L., 2005. Phosphate removal
556 from the returned liquor of municipal wastewater treatment plant using iron-reducing
557 bacteria. J. Appl. Microbiol. 98, 1152–1161. https://doi.org/10.1111/j.1365-
558 2672.2005.02567.x

559 Jardin, N., Pöpel, H.J., 2001. Refixation of phosphates released during bio-p sludge handling

560 as struvite or aluminium phosphate. Environ. Technol. 22, 1253–1262.
561 https://doi.org/10.1080/09593332208618193

562 Jurtshuk, P., 1996. Bacterial Metabolism, in: Samuel Baron (Ed.), Medical Microbiology.
563 Galveston (TX): University of Texas Medical Branch at Galveston.

564 Le Corre, K.S., Valsami-Jones, E., Hobbs, P., Parsons, S. a., 2005. Impact of calcium on
565 struvite crystal size, shape and purity. J. Cryst. Growth 283, 514–522.
566 https://doi.org/10.1016/j.jcrysgro.2005.06.012

567 Leng, Y., Colston, R., Soares, A., 2020. Understanding the biochemical characteristics of
568 struvite bio-mineralising microorganisms and their future in nutrient recovery.
569 Chemosphere 247, 125799. https://doi.org/10.1016/j.chemosphere.2019.125799

570 Logan, B.E., 2008. Kinetics and mass transfer, in: Microbial Fuel Cells. John Wiley & Sons,
571 Inc. https://doi.org/10.1002/9780470258590.ch7

572 Logan, B.E., 2005. Cellular growth and reproduction, in: Structural and Functional
573 Relationships in Prokaryotes. Springer, New York, pp. 292–347.
574 https://doi.org/https://doi.org/10.1007/0-387-27125-2_7

575 Mann, S., 2001. Biomineralization : principles and concepts in bioinorganic materials
576 chemistry. Oxford University Press.

577 Mijangos, F., Kamel, M., Lesmes, G., Muraviev, D.., 2004. Synthesis of struvite by ion
578 exchange isothermal supersaturation technique. React. Funct. Polym. 60, 151–161.
579 https://doi.org/10.1016/J.REACTFUNCTPOLYM.2004.02.019

580 Mindat, 2018. Struvite [WWW Document]. Mindat.org. URL https://www.mindat.org/min-
581 3811.html (accessed 2.5.20).

582 Nocker, A., Cheswick, R., Dutheil de la Rochere, P.M., Denis, M., Léziart, T., Jarvis, P., 2017.
583 When are bacteria dead? A step towards interpreting flow cytometry profiles after chlorine
584 disinfection and membrane integrity staining. Environ. Technol. 38, 891–900.
585 https://doi.org/10.1080/09593330.2016.1262463

586 Omar, N. Ben, Gonzalez-Muñoz, M.T., Peñalver, J.M. a, 1998. Struvite crystallization on
587 Myxococcus cells. Chemosphere 36, 475–481. https://doi.org/10.1016/S0045-
588 6535(97)10014-5

589 Orange, F., Westall, F., Disnar, J.R., Prieur, D., Bienvenu, N., Le Romancer, M., DÉfarge, C.,

2009. Experimental silicification of the extremophilic Archaea Pyrococcus abyssi and Methanocaldococcus jannaschii: applications in the search for evidence of life in early Earth and extraterrestrial rocks. Geobiology 7, 403–418. https://doi.org/10.1111/j.1472-4669.2009.00212.x

Prywer, J., Torzewska, A., Płociński, T., 2012. Unique surface and internal structure of struvite crystals formed by Proteus mirabilis. Urol. Res. 40, 699–707. https://doi.org/10.1007/s00240-012-0501-3

Ratke, L., Voorhees, P.W., 2013. Growth and coarsening: Ostwald ripening in material processing. Springer Science & Business Media.

Sadowski, R.R., Prywer, J., Torzewska, A., 2014. Morphology of struvite crystals as an evidence of bacteria mediated growth. Cryst. Res. Technol. 49, 478–489. https://doi.org/10.1002/crat.201400080

Schultze-Lam, S., Fortin, D., Davis, B., Beveridge, T., 1996. Mineralization of bacterial surfaces. Chem. Geol. 132, 171–181. https://doi.org/10.1016/S0009-2541(96)00053-8

Shaddel, S., Ucar, S., Andreassen, J.P., Sterhus, S.W., 2019. Engineering of struvite crystals by regulating supersaturation - Correlation with phosphorus recovery, crystal morphology and process efficiency. J. Environ. Chem. Eng. https://doi.org/10.1016/j.jece.2019.102918

Simoes, F., 2017. A new route to recover phosphorus from waste water: biological struvite production School. Cranfield University.

Simoes, F., Vale, P., Stephenson, T., Soares, A., 2017. Understanding the growth of the bio-struvite production Brevibacterium antiquum in sludge liquors. Environ. Technol. 1–10. https://doi.org/10.1080/09593330.2017.1411399

Sinha, A., Singh, A., Kumar, S., Khare, S.K., Ramanan, A., 2014. Microbial mineralization of struvite: a promising process to overcome phosphate sequestering crisis. Water Res. 54, 33–43. https://doi.org/10.1016/j.watres.2014.01.039

Smirnov, A., Suzina, N., Chudinova, N., Kulakovskaya, T., Kulaev, I., 2005. Formation of insoluble magnesium phosphates during growth of the archaea Halorubrum distributum and Halobacterium salinarium and the bacterium Brevibacterium antiquum. FEMS Microbiol. Ecol. 52, 129–137. https://doi.org/10.1016/j.femsec.2004.10.012

Soares, A., Veesam, M., Simoes, F., Wood, E., Parsons, S. a., Stephenson, T., 2014. Bio-Struvite: A new route to recover phosphorus from wastewater. Clean - Soil, Air, Water 42, 994–997. https://doi.org/10.1002/clen.201300287

Spiegel, C.N., Bretas, J.A.C., Peixoto, A.A., Vigoder, F.M., Bruno, R. V., Soares, M.J., 2013. Fine structure of the male reproductive system and reproductive behavior of Lutzomyia longipalpis sandflies (Diptera: Psychodidae: Phlebotominae). PLoS One 8, e74898. https://doi.org/10.1371/journal.pone.0074898

Stolp, H., 1988. Microbial ecology: organisms, habitats, activities. Cambridge University Press.

Tansel, B., Lunn, G., Monje, O., 2018. Struvite formation and decomposition characteristics for ammonia and phosphorus recovery: A review of magnesium-ammonia-phosphate interactions. Chemosphere 194, 504–514. https://doi.org/10.1016/j.chemosphere.2017.12.004

Weiner, S., Dove, P.M., 2003. An overview of biomineralization processes and the problem of the vital effect, in: Reviews in Mineralogy and Geochemistry. pp. 1–29. https://doi.org/10.2113/0540001

Westall, F., 1999. The nature of fossil bacteria: A guide to the search for extraterrestrial life. J. Geophys. Res. 104451, 437–16. https://doi.org/10.1029/1998JE900051

Yee, N., Phoenix, V.R., Konhauser, K.O., Benning, L.G., Ferris, F.G., 2003. The effect of cyanobacteria on silica precipitation at neutral pH: Implications for bacterial silicification in geothermal hot springs. Chem. Geol. 199, 83–90. https://doi.org/10.1016/S0009-2541(03)00120-7



https://dspace.org/

Understanding the mechanisms of biological struvite biomineralisation

Leng, Yirong; Soares, Ana

2021-10-1
Elsevier
https://doi.org/10.1016/j.chemosphere.2021.130986
Leng Y, Soares A. (2021) Understanding the mechanisms of biological struvite biomineralisation. Chemosphere, Volume 281, October 2021, Article number 130986

Downloaded from a DSpace repository. https://dspace.org/